ARTICLE

Graphene oxide-Au nano particle coated quartz crystal microbalance biosensor for the real time analysis of carcinoembryonic antigen

Received 00th January 20xx,
Accepted 00th January 20xx

DOI: 10.1039/x0xx00000x

P J Jandas[a,b], Jingting Luo[a]*, Aojie Quan[a], Chong Li[a], Chen Fu[a]*,Y Q Fu[c]

Abstract

A label-free quartz crystal microbalance (QCM) biosensor was developed for the selective and real-time estimation of carcinoembryonic antigen (CEA) through the present study. Graphene oxide – Au nanoparticles (GO-AuNP) was in-situ synthesised on the surface of the QCM electrode and antibody of CEA (monoclonal anti-CEA from mouse) was covalently immobilized on this layer as the bioreceptor for CEA. Mercaptoacetic acid – EDC-NHS reaction mechanism was used for the anti-CEA immobilization. The effect of oxygen plasma treatment of the QCM electrode surface before the bioreceptor preparation on the performance of the biosensor was tested and find promising. CEA solutions with various concentrations were analysed using the bioreceptors to estimate the sensitivity and detection limit of the biosensor. The biosensors were selectively recognized and captured CEA biomolecules with a detection limit of 0.06 and 0.09 ng/ml of CEA for oxygen plasma-treated (E2) and untreated (E1) bioreceptors respectively. The sensitivity was estimated at 102 and 79 Hz respectively for E2 and E1. Clinical serum samples were analysed and the results were found in good agreement with the ELISA analysis. Long term stability was also found excellent. Langmuir adsorption isotherm was conducted using the experimental results as well.

1. Introduction

Abnormally high level of carcinoembryonic antigen (CEA) in the human body is often referred to the presence of cancer in any of the organs including colon, breast, lungs, gastric and ovary.[1] Average level of CEA in a healthy human body is 5µg/L. Any value of CEA higher than 20 µg/L is considered as an alarm signal for the presence of tumour cells in the body. A rapid, accurate and periodical detection of the CEA concentration provides helpful information about the stage, progression and recurrence of a cancer.[2] Majority of present methods use antigen (analyte) and antibody (the receptor system) based detection strategy with detectors based on colorimetry, fluorescence, chemiluminescence, electrochemical, surface-enhanced Raman scattering etc.[3,4]

However, sensitivity of many of these devices is a critical issue. The popular methods such as enzyme-linked immunosorbent assay (ELISA), radioimmunoassay and Raman readouts have potential problems such as low sensitivity, long detection time, safety issues and reproducibility of the results. Electrochemical methods are studied extensively, but the methods demand complicated labelling process to ensure high sensitivity.[5,6] This makes the method labour-intensive and sometimes labelling may hinder the activity of biomolecules also. In this perspective, label-free, highly sensitive, safe and real-time analysis of tumour markers is still an active challenge for researchers.

Piezoelectric biosenosrs such as surface acoustic wave (SAW) sensors and quartz crystal microbalance (QCM) sensors are popular today.[7] QCM is a priority tool for biomolecular analysis because of its unique advantages like high sensitivity, low response time, easy operation, portable device, cost-effectiveness and label-free and real-time detection ability.[8] The QCM electrode consists of a quartz electrode sandwiched by metal (Au, Al, Ti etc) layers for electrical contact. Any mass deposition on the electrode tends to change the frequency response of the crystal. This can be detected by an analyser system with high accuracy.[9] The QCM based biosensors are popular for the analysis of DNA molecules.[10], proteins.[11], cancer diagnosis and tumour marker detection.[12], differentiation between cancerous and normal cells.[13] Chen and Tang have presented a QCM based biosensor for the detection of CEA based on a bioreceptor prepared through non-covalent based interactions.[14] Yang *et al.* have described a QCM based CD44 biosensor for the analysis of the metastatic potential of breast cancer cells.[15] Recently Uludag and Tothill reported a systematic approach to the human serum sample

1Shenzhen Key Laboratory of Advanced Thin Films and Applications, College of Physics and Energy, Shenzhen University, 518060, Shenzhen, PR China

Email: luojt@szu.edu.cn; chenfu@szu.edu.cn

2Key Laboratory of Optoelectronic Devices and Systems of Ministry of Education and Guangdong Province, College of Optoelectronic Engineering, Shenzhen University, 518060, Shenzhen, PR China

3Faculty of Engineering and Environment, Northumbria University, Newcastle upon Tyne, NE1 8ST, UK

analysis for tumour markers using QCM.[16] Detection of *E.coli* O157: H7 was reported by Yu *et al.* suggested the effectiveness of the QCM tool for the detection of microorganisms too.[17] Another recent notable investigation in QCM based biosensors was by D. Tang.[18] The study has illustrated a systematic method for the determination of tumour necrosis factor alpha using the piezoelectric biosensor.

In the present study, a QCM based biosensor was prepared for the detection of CEA with good selectivity, sensitivity, stability and reproducibility. Immobilization of anti-CEA on the QCM electrode surface is the vital and challenging part of the biosensor fabrication process. This is because the bioreceptor surface needs to act like an active and selective host for the CEA molecules from the analyte sample. This is possible only if we can immobilize a uniform anti-CEA layer on the QCM electrode surface. The study presents a novel method for bioreceptor preparation using a nanomaterial cluster of GO-AuNP. The GO flacks are proven materials for biosensing by providing easy transduction of signals from biochemical reactions to electrode outputs.[19,20] AuNP can act like a reaction nucleus for the immobilization of anti-CEA by creating a covalent based interaction with the sulphur atom of mercaptoacetic acid. A range of CEA concentration from 0.1 ng/ml to 120 ng/ml was used for immunoassay analysis in the present study. The mass of CEA deposited on the SAM was calculated using modified Souerbrey's equation for liquid state analysis.

2. Experimental

2.1. Materials and instruments

All the chemicals and biological samples including cancer-associated carcinoembryonic antigen (CEA), CEA monoclonal antibody (anti-CEA) produced in mouse, alpha-1-fetoprotein (AFP, Monoclonal Anti-α-Fetoprotein produced in mouse) and L-tryptophan ((S)-2-amino-3-(3-indolyl)propionic acid), bovine serum albumin (BSA, 96-99%), mercaptoacetic acid, Ethyl-dimethyl-aminopropyl carbodiimide (EDC), N-Hydroxy succinimide (NHS), sodium citrate, HAuCl4.3H2O and all other common reagents were purchased from Sigma Aldrich, USA. Cancer antigen 125 (CA125, Biotinylated Human CA125 / MUC16 Protein, Fc, Avitag) was purchased from Biosystem ACRO, USA. Clinical serum samples were supplied by Second People's Hospital, Shenzhen, China. The samples were collected from the patients who were suspected to affect by colorectal cancer. Buffer solution with pH 7.4 was prepared using K2HPO4 and KHPO4. BSA solution with concentration 10 mg/ml was prepared and used. Both the solutions were prepared freshly for each use. CEA solutions of concentrations 0.1 ng/ml to 100 ng/ml were prepared in PBS solution and stored in the sterile conditions. CEA sample obtained was tested for activity using ELISA method.

QCM with impedance measurement (QCM-I, MicroVacuum Ltd, Hungary) with electrode consists of AT cut optically polished circular quartz crystal (15 mm diameter, TiAuTi) was used for the measurements. The basic resonant frequency of the crystal was 5MHz and the frequency shift of the normalized 5th overtone was used to quantify CEA during immunoassay experiments.

2.2. Electrode pre-treatment and bioreceptor preparation

QCM electrode crystal was cleaned by sonication in ethanol for 10 minutes. The surface was degreased using piranha solution (1:3 H2O2: H2SO4) for 20 minutes, followed by washing in deionised water (DI water) and ethanol. The surface was then dried at 80°C in a vacuum oven under nitrogen flow. 0.05g of GO was taken in a beaker containing 5 ml of DI water. The mixture was heated to 80°C and added 2.50 ml of 10.35 mg/ml of sodium citrate followed by 1 ml of 5 mg/ml aqueous solution of HAuCl4.3H2O. The resulting precursor solution was sonicated for 5 minutes and placed 1 mL of the solution on the QCM electrode surface. The electrode was further incubated in a vacuum oven for 30 minutes at 80°C under nitrogen atmosphere. The nanoparticle coated electrode was cooled using an ice bath washed with DI water, followed by ethanol. SEM and TEM and AFM images of the surfaces were taken to understand the morphology. Further, thioglycolic acid (5mM) was introduced to the GO-AuNP surface and allowed to react for 2 hours. The surface washed in ethanol, followed by using DI water and dried under nitrogen flow. 2 mL solution mixture of 400 mM EDC and 100 mM NHS (1:1 v/v) in methanol was allowed to react with the surface in the next stage. In the next step, the surface was treated with 100 µg/mL of capture monoclonal anti-CEA and incubated at 4°C and 50±5% relative humidity for 12 hours. The concentration of monoclonal anti-CEA was optimized through QCM analysis after immobilization with various concentrations and theoretical calculation of fractional coverage of electrode surface (results are given in the supportive data, Table S4). The surface was cleaned with PBS solution and dried under nitrogen flow after the incubation period. The electrode crystals stored at 4°C and 50±5% under sterile conditions to avoid any contaminations. The bioreceptor surface was characterized using scanning electron microscopy (SEM, Zeiss EVO-MA), atomic force microscopy (Bruker NanoWizard®4), optical/fluorescence microscopy (Ningbo Sunny Technology Co. Ltd, CX40 Biological optical/fluorescence microscope) and contact angle study (United Test Co., Ltd, CAG100 Contact Angle Goniometer).

Oxygen plasma treatment

The chemically cleaned Au surface using piranha solution was treated with O2 plasma using RGC-100 Series Digital Vacuum Gauge, Agilent Technologies. The power of oxygen plasma and time of exposure was optimized at 120 Watts and 10 minutes respectively. Immediately after the plasma exposure, the surface underwent bioreceptor preparation processes as discussed in the above section. The hypothesis behind oxygen plasma treatment was the ionized oxygen can activate the electrode surface and provide good adhesion with nanomaterial cluster. The plasma treatment may also tend to provide better effective surface area for the bioreceptor preparation and potential reaction sites as compared with the untreated QCM electrode surface.

2.3. Biosensing using QCM

The frequency shift of each immunoassay run was recorded as a function of response time at an interval of 5 seconds using a data acquisition system connected to a computer with the QCM instrument. The flow rate of the sample for the entire experiment was optimized as 0.05 ml/minute. Newly prepared biosensors were treated with BSA before immunoassay runs to minimize the unwanted adsorptions. Fixed volumes of CEA solutions with variable concentrations ranging from 0.1 ng/ml to 120 ng/ml and allowed to flow through the receptor cell of QCM instrument till a stable plateau obtained. End of each immunoassay analysis the bioreceptor was washed with PBS solution. Final average values of equilibrium frequency shift with standard deviation are reported in the study.[21] After each immunoassay measurement, regeneration of the SAM was conducted by running a buffer solution of HCl (0.8M), KCl (0.06 M) and glycine 0.06 M for half an hour or till getting a stable plateau. Frequency shift was converted to the amount of CEA deposited on the bioreceptor through the calculation using modified Sauerbrey's equation for liquid phase experiments.[22-24]

TEM figures of GO and GO-AuNP are given in the figure 1a and 1b. The 2D single layers of GO prepared through modified Hummer's method are clearly detectable from the TEM figure. The separate layers of GO has an average surface dimension of 40 x 60 nm. AuNP of dimension around 5-10 nm were found formed on the GO layers as given in figure 1b. The brighter spots on the GO layers represent the AuNP. This has been further confirmed using SEM figures. The SEM figures of GO-AuNP coated QCM electrodes are given in the figure 2 (a-c). Figure 2a represents the surface of piranha treated QCM electrode. Figure 2b and 2c represent GO-AuNP coated surfaces of E1 and E2 respectively. Well formed AuNP on the GO layers are visible within the figures and number density of the particles found better on the E2 electrode than that of E1. Oxygen plasma may enhance the energy state of the Ti coated electrode surface and may provide better adhesion for the nanoparticles during the in-situ formation process. This may be the reason for better particle density on E2 electrode surface.

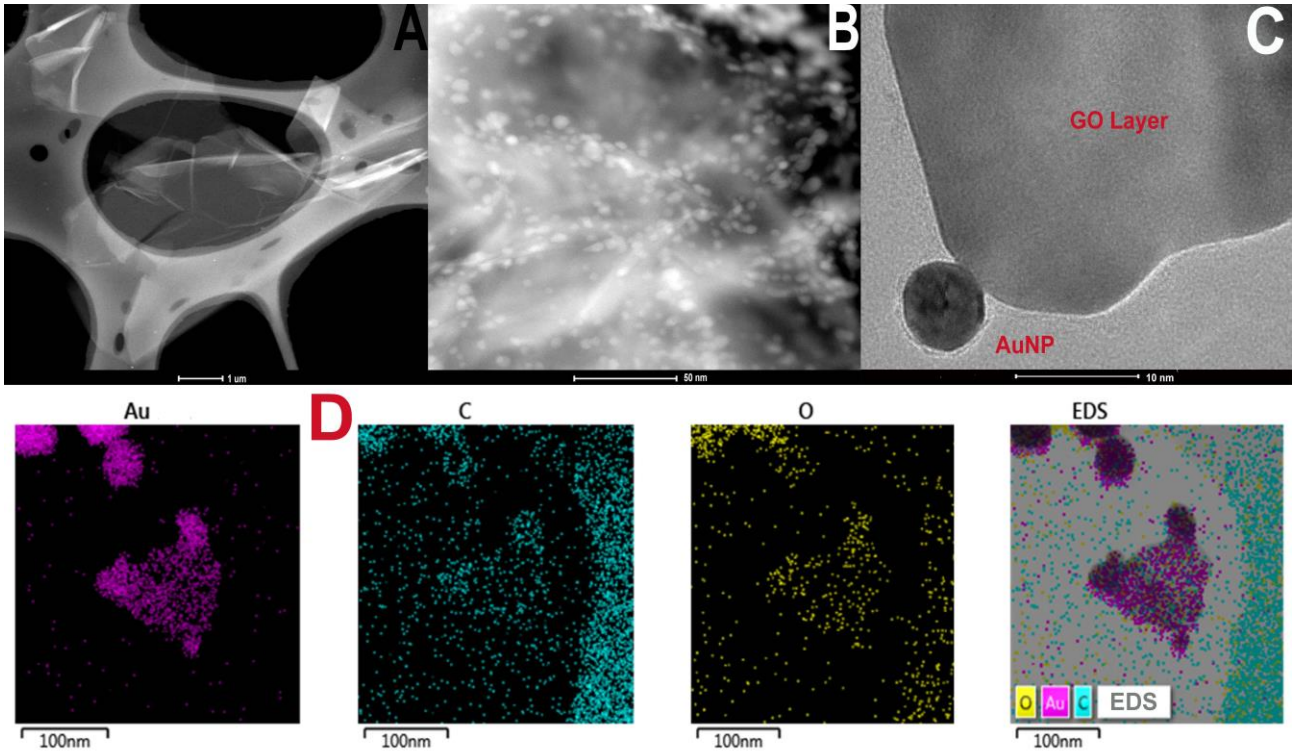

Figure 1(A) TEM of Graphene oxide sysnthesised by modified Hummer's method **(B & C)** TEM of GO-AuNP synthesised in the present study **(D)** TEM-EDS elemental mapping of GO-AuNP

3. Results and discussions

3.1. Characterization of nanomaterials coated QCM surface

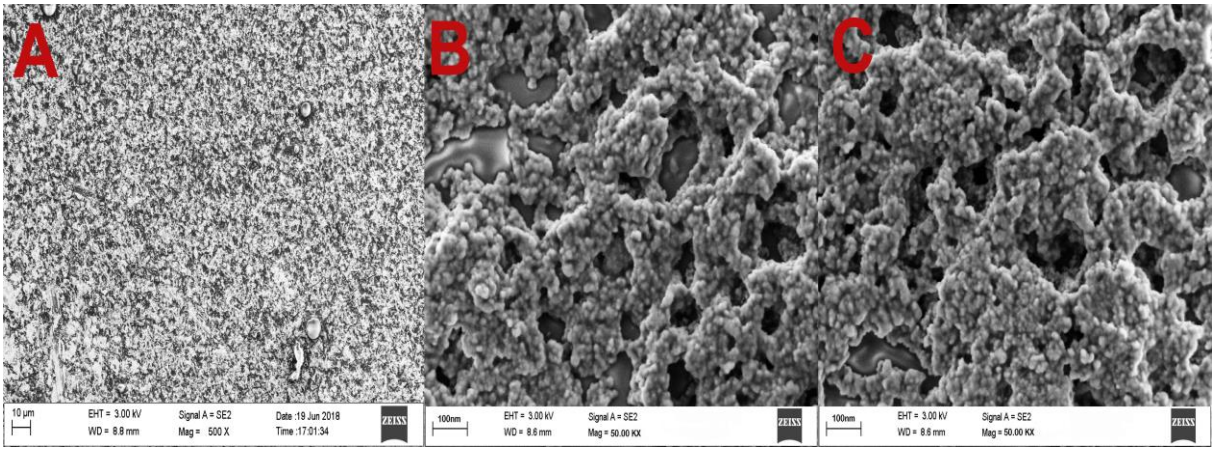

Figure 2 (A) Surface morphology of piranha treated QCM electrode **(B)** GO-AuNP synthesised on the QCM electrode E1 and **(C)** GO-AuNP synthesised on the QCM electrode E2

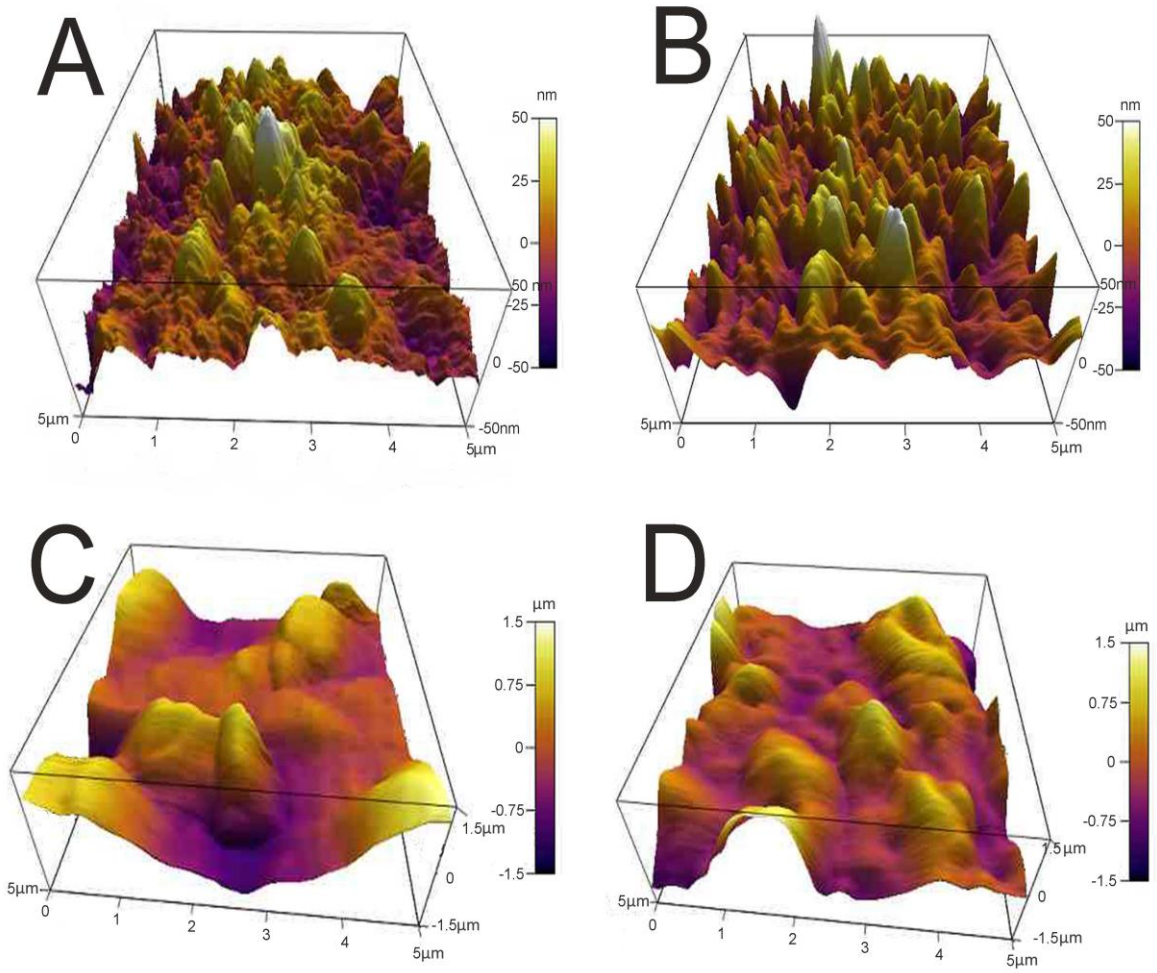

Figure 3(A) E1 electrode after the coating of GO-AuNP **(B)** E2 electrode after the coating of GO-AuNP **(C)** E1 electrode after the bioreceptor preparation (D) E2 electrode after the bioreceptor preparation

AFM analysis provides additional evidence to the formation of the GO-AuNP coating on the QCM electrode as given in the Figure 3a and b. The AFM figures were given an idea about the thickness of the thin film of nanoparticles formed on the electrode surfaces. An average of 50 nm thickness was observed for both the methods of electrode preparations. The pillars like structures in the AFM images represent the coated nanoparticles on the surface. The thickness of the nanoaparticle layers suggests 3-4 GO-AuNP layers were deposited on the electrode surface.

3.2. Characterization of self assembled monolayer (SAM) bioreceptor

The bioreceptor preparation steps were monitored using QCM analysis to study the deposition of nanomaterial and biomolecular film on the electrode surface. Figure 4a, represents the frequency response towards PBS run, before and after the SAM preparation for E1 and E2 electrodes. After the GO-AuNP thin film coating the frequency shift of E2 has changed to an average value of around -165 Hz and after the immobilization of Anti-CEA to around -15623 Hz. E1 has responded to the PBS solutions at -111 Hz and -13567 Hz respectively after GO-AuNP thin film coating and anti-CEA immobilization. The reduced frequency shift is pointing out to the successful addition of GO-AuNP thin film and immobilization of anti-CEA bioreceptor film on the surface of QCM electrode crystal. The higher deviation in frequency in case of E2 than E1 is due to the better wetting of QCM electrode surface towards nanoparticles after oxygen plasma treatment. More the number of AuNP on the surface ultimately provides higher numbers of reaction sites to immobilize anti-CEA molecules. The high energy plasma particles may activate the Ti atoms from the electrode surface and can adhere with larger number of reaction nanoparticles than that of the normal conditions. This may end up in denser anti-CEA film on the bioreceptor surface.

SEM images of E1 and E2 (Figure 5 a and b respectively) displayed a well formed new layer of SAM on the electrode crystal. The rough morphology of nanomaterial coated electrode crystal has been covered with a thin film of biological molecules based SAM. The magnified figures of each surface (60 KX) are given in the Figure 5(c and d). Individual reaction nuclei created by the immobilization of Anti-CEA are visible in the figures. The number of reaction nuclei on the bioreceptor surface has observed higher for E2 as compared to E1. AFM images also suggest the formation of a new layer of SAM on the surface of QCM electrode which is depicted in Figures 3(c and d) respectively for E1 and E2. The topographic images of E1 and E2 have many 'ups and downs' is due to the presence of immoblized Anti-CEA molecules. The thickness of the newly formed layer is of around 1000-1200 nm, which suggests the formation of a monolayer of anti-CEA molecules on the bioreceptor surface.

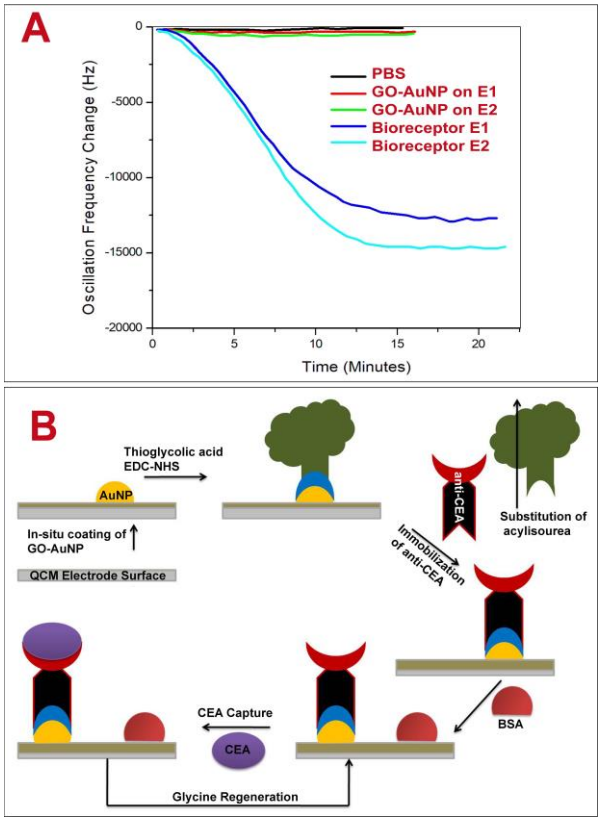

Figure 4(A): Frequency shift of QCM after GO-AuNP coating and bioreceptor preparation PBS flow (pH – 7.4) at room temperature. **(B)** Scheme of biosensing used in the present study

Thioglycolic acid has the capability to interact with the AuNP on surface of electrode crystal with stable chemical and physical bonds. According to T. Bürgi, sulphur molecules can form coordination bonds with the transition metals elements.[25] The vacant outermost orbital of Au can interact with lone pairs of sulphur to form stable coordination linkage in between the AuNP on the electrode crystal surface and thioglycolic acid. The maximum bond energy reported as for S-Au linkage is 184 $kJmol^{-1}$.[25] Further, the thin layer of carboxylic acid terminated thioglycolic acid can be activated through EDC-NHS coupling agent to form semi-stable acylamino ester intermediates as given in Figure 6 a-b. This acylamino ester groups can interact with the primary amine groups of Anti-CEA molecules to undergo substitution reaction to form a covalently bonded stable bioreceptor for CEA capture.

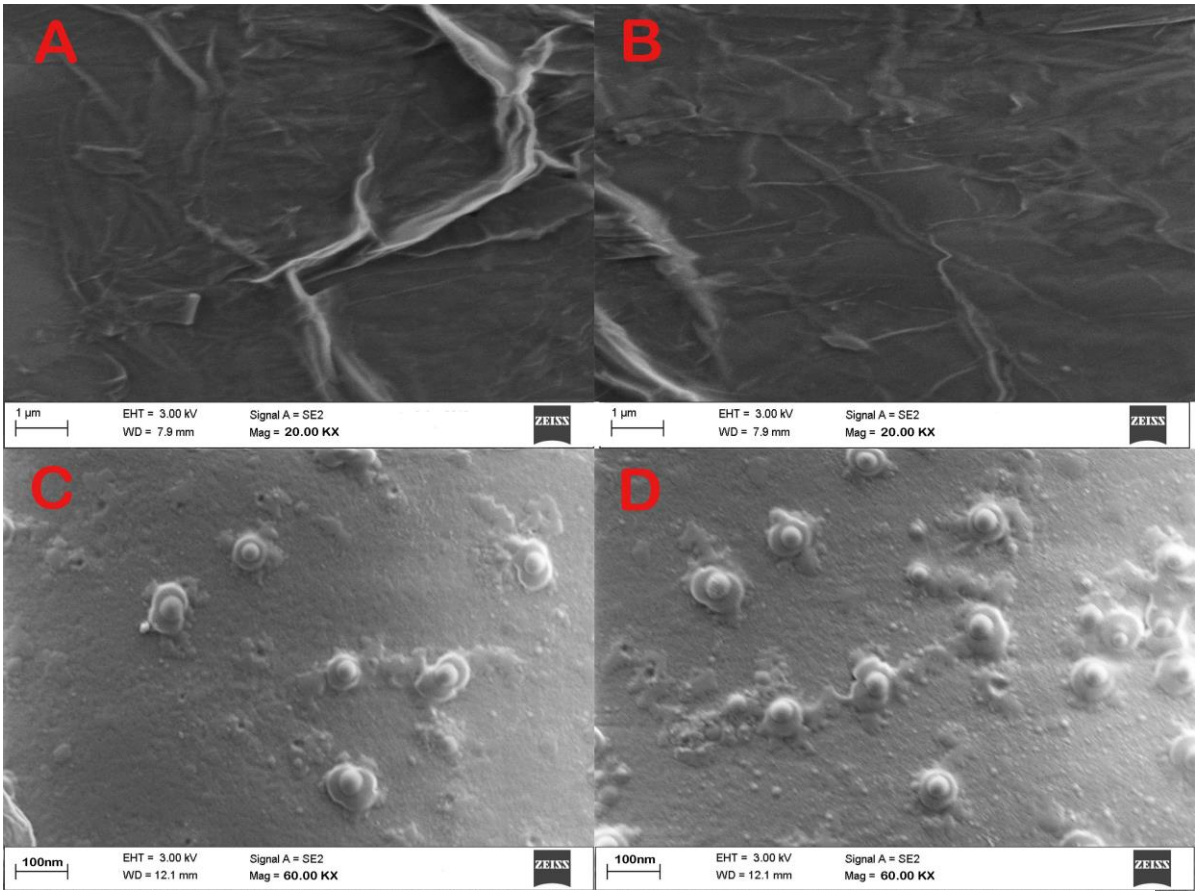

Figure 5 (a) and **(b)** Morphology of bioreceptor prepared on E1 and E2 **(c)** and **(d)** Magnified morphology of E and E2

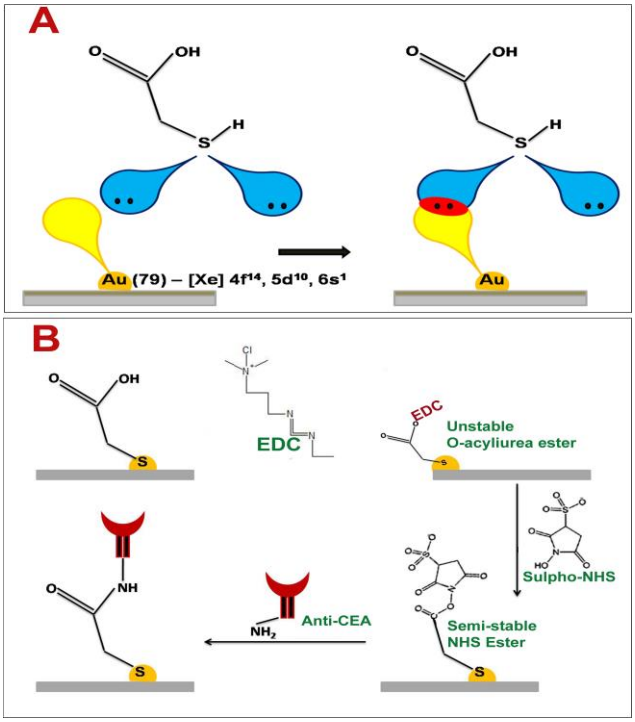

Figure 6 (A): The interactive pattern of AuNP and thioglycolic acid **(B)** The chemistry behind the anti-CEA

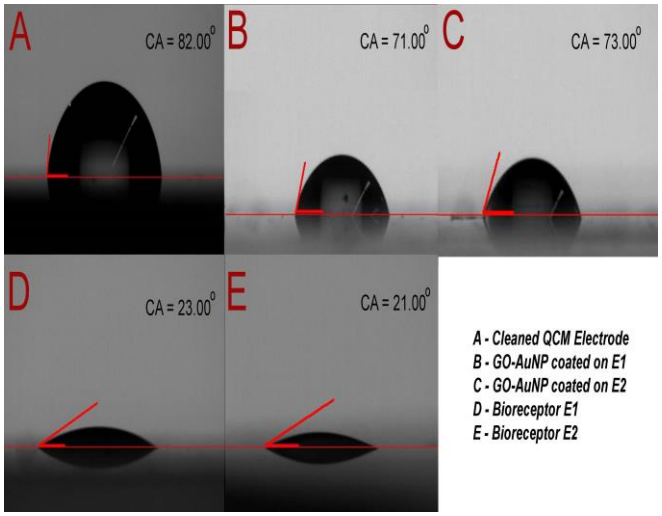

Figure 7(a) Contact angle of piranha cleaned QCM electrode surface **(b)** Contact angle of E1 surface after GO-AuNP coating **(c)** Contact angle of E2 surface after GO-AuNP coating **(d)** E1 bioreceptor after anti-CEA immobilization **(e)** E2 bioreceptor after anti-CEA immobilization

The immobilization of anti-CEA also has an effect on the hydrophilic characteristics of the electrode surface. The same has characterized and results depicted in Figure 7. The clean Au surface had a contact angle of 82°, which is reduced to 71 and 73 after nanomaterial coating and further reduced to 23° and 21° after anti-CEA immobilization respectively for E1 and E2. Presence of polar, hydrophilic biological molecules tends to enhance the hydrophilicity of the electrode surface after the formation of the bioreceptor. This is further confirms the successful formation of biofilm on the QCM electrode surface through the method used in the present study.

3.3. Immunoassay run for CEA solutions

Biosensing capability and limit of detection of the newly prepared biosensors was estimated by performing a series of immunoassay run with different stock solutions of CEA prepared in PBS at pH 7.4. The general principle of biosensing of CEA in the present research is depicted in Figure 4b. The prepared biosensor was treated with BSA solution prior to the immunoassay experiments to reduce the non-specific adsorption of CEA. Multiple immunoassay runs were conducted for each concentration of CEA stock solution and the representative image of the immunoassay response of biosensors are depicted in Figure 8a and 9a respectively for E1 and E2. Corresponding average values of variation in frequency response for each CEA concentrations from the base frequency of the respective biosensors are given in Figure 8b and 9b (standard deviations (S.D.) are shown as error bars). The calibration curve as log-log plots to determine the lower and upper limit of detection are given in the Figure 8c and 9c. The final value of frequency shift has obtained after PBS washing at the end of each immunoassay run. The bioreceptor E2 was responded linearly with the increase in the concentration of CEA, as the frequency response decreased from 0.1 ng/ml CEA to 120 ng/ml. Immunoassay experiment has conducted for 0.01ng/ml CEA as well. However, the solution cannot create any considerable variation in the base frequency of the biosensor E2. Hence, the corresponding frequency response is not given in the figure. The biosensor E2 was responded to 0.1 ng/ml of CEA with variation in equilibrium frequency from the base frequency of around -12.5 Hz. Further, the frequency shifted to lower side consistently with increasing CEA concentration and a maximum value of deviation in frequency at -13260 Hz was recorded for 120 ng/ml. Similarly, biosensor E1 also responded to the CEA stock solutions (Figure 4a and 4c) however, the values are comparably lower to that of E2 for each concentration of CEA stock solutions. The E1 bioreceptor responded to 0.1 ng/ml stock solutions with an oscillation frequency of 8.5 and 7120 Hz for 100 ng/ml solution. Oxygen plasma treatment at the beginning of bioreceptor preparation may end up with a better effective area for bioreceptor and better accessibility for prey CEA molecules during immunoassay run, thereby lower oscillation frequency. As expected, the Ti atoms may get excited to an energetically higher state under oxygen plasma and more number of nanoparticles may adhere on the surface. Higher number of AuNP can react with thioglycoclic acid which ultimately creates more reaction sites for CEA immobilization as compared with the untreated one. This may tends to create better effective surface for the biorecetor E2 with more number of immobilized anti-CEA molecules than E1. This may be the reason for higher frequency shift for E2 than E1 during immunoassay analysis.

The response time of the bioreceptor also found good and comparable or better than some of the reported values by various researchers.[26-29] In the present study, the equilibrium plateau is attained for each immunoassay run within a minimum time period of 15-30 minutes. The limit of detection for both the biosensors was calculated as blank frequency response by PBS + 3 × Noise (standard deviation).[30] The detection limit of E1 was calculated as 0.45 ng/ml of CEA concentration and that of E2 with a better value of 0.33 ng/ml. Upper saturation points of the biosensors was calculated from the log-log plots and for E1 the value obtained around 91ng/ml and that for E2 at 113 ng/ml. The LOD values are better than the many of the reported studies and a comparison with some of the piezoelectric biosensors for CEA detection is given in the supportive data as Table S2. The performance of both the biosensor methods was also evaluated through the calculation of total mass deposition on the electrode crystal using experimental values and theoretical calculation using the concentration CEA solutions. Since the known concentrations of solutions used for the immunoassay run, the weight of total CEA in each sample was calculated for the total flow of sample and obtained values compared with the experimental results achieved through modified Sauerbrey's equation. The comparison is listed in Table S1 as supportive data. According to the values obtained, the accuracy of the biosensor found good and the results show less than 10% deviation from the theoretical values. The sensitivity of the biosensors was calculated using Sauerbrey's equation and found impressive values at 87 and 123Hz/ng of CEA respectively for E1 and E2. The reproducibility study was conducted as per the studies reported by M. Y. Emran et al.[31-34] The results found good with both the bioreceptors. Both the bioreceptors didn't show much difference in performance till 8th immunoassay run and further the frequency shift started deteriorating. The average values of variation in immunoassay response as a function of reproducibility are given in Figure S1.

3.4. Sorption equilibrium of CEA on the bioreceptor sensing interphase

Langmuir isotherm was used to understand the favourable nature of the adsorption of CEA on the bioreceptor. Experimental data fit well with the Langmuir adsorption isotherm as depicted in Figure 10a and 10b for both E1 and E2 respectively. A liner fit for k_{obs} versus C, for both E1 and E2 suggests that the sorption follows Langmuir adsorption isotherm. The isotherm enables to calculate the kinetic constants of adsorption (k_a) and desorption (k_d) as 2991 ± 524L mol^{-1} s^{-1} and 6.83 ± 1.81) × 10^{-4} s^{-1}, respectively as the slope and intercept of the graph for E1. A non-zero value for k_d implies an existing equilibrium within the A-CEA – CEA interface. E2, on the other hand, the most significant

observation noted is that the low k_d (8.95 ± 1.75× 10^{-5} s^{-1}) value and an increased k_a (3672 ± 341$Lmol^{-1}s^{-1}$) as compared to the untreated immunoassay samples. This further suggests an increased activity of bioreceptor interface through oxygen plasma treatment and shifted equilibrium of anti-CEA – CEA interaction more towards the forward reaction side (association). In other words, equilibrium attained with reduced dissociation rate may be due to the stronger anti-CEA – CEA interaction facilitated by the increased stability of bioreceptor of E2.

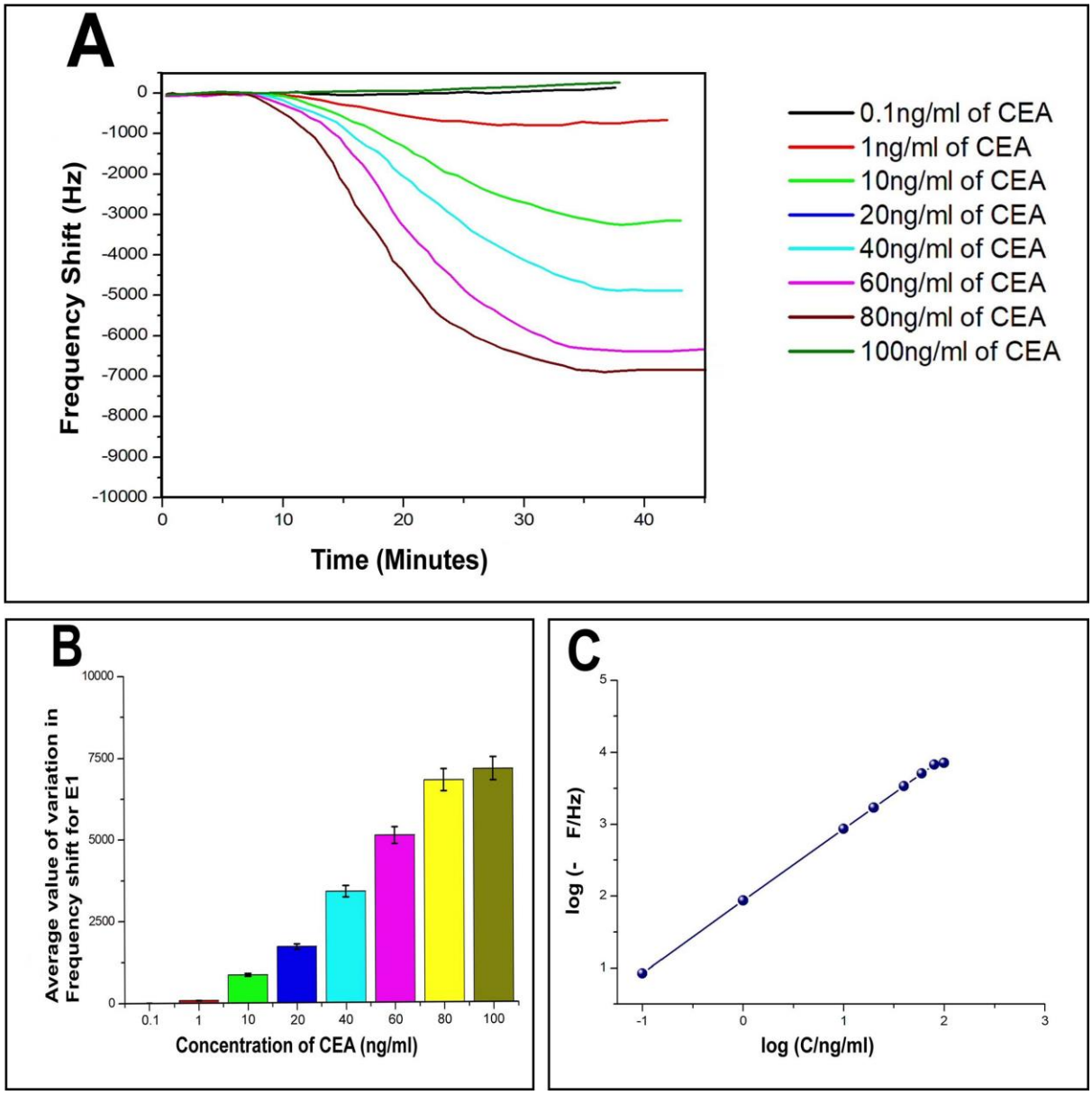

Figure 8(a) immunoassay response of E1 **(b)** Average value of variation in oscillation frequency from base value of E1 **(c)** calibration curves of E1

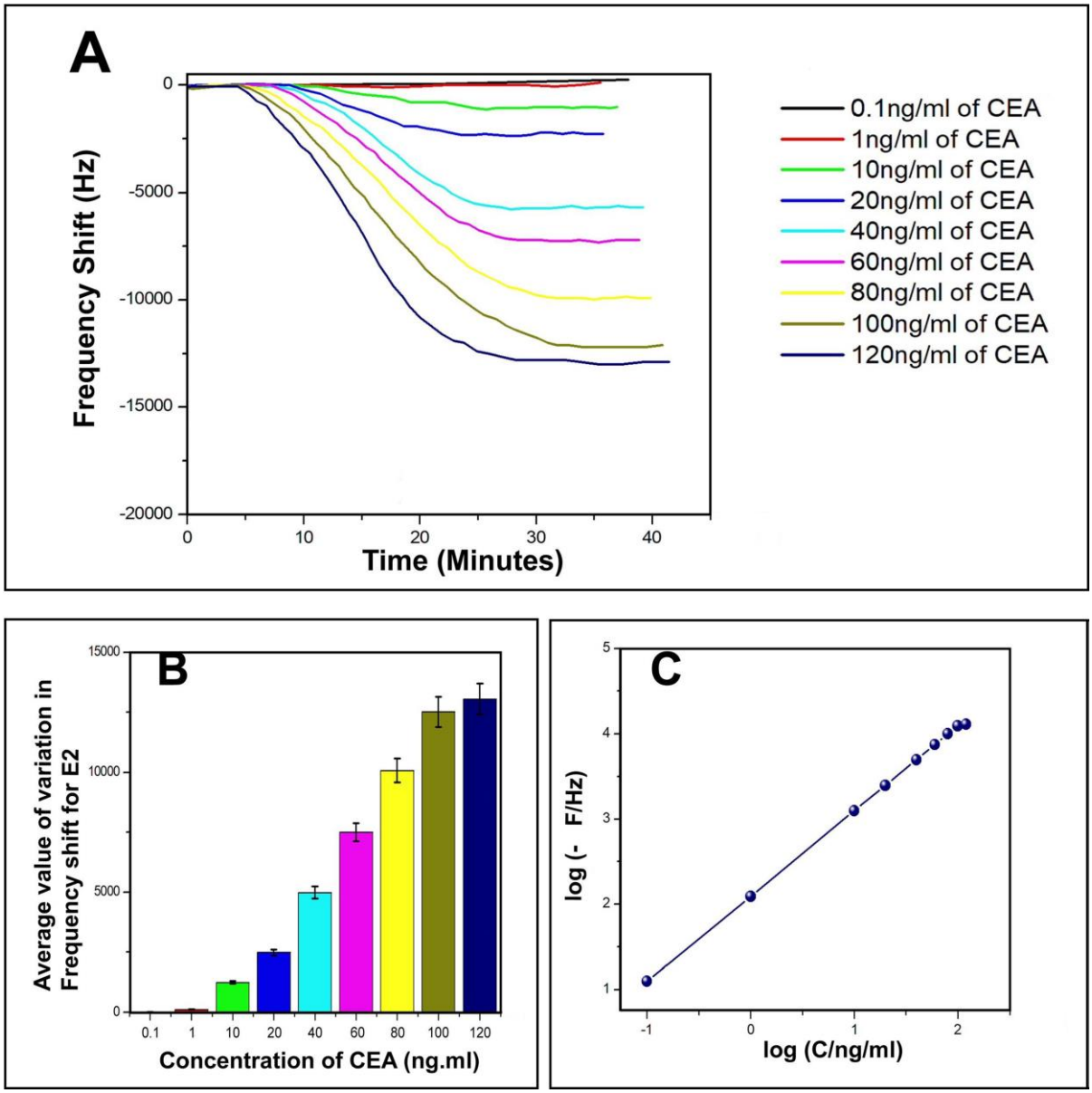

Figure 9(a) immunoassay response of E2 **(b)** Average value of variation in oscillation frequency from base value of E2 **(c)** calibration curves of E2

The observations from isotherm study are in good correlation with the frequency response study as discussed in the prior section, since considerably higher depression in frequency for oxygen plasma treated electrode crystal, E2, than that of its untreated counterparts, E1. The better interaction with bioreceptor and ligand may tend to reduce the rate of backward reaction. This can end as a higher equilibrium deposited mass on E2 and the corresponding increase in frequency shift towards more negative side.

Also, the free energy of sorption process calculated and negative values for E1 and E2 were recorded. However, $\Delta G_{sorption}$ for E2 is observed as a higher negative value than that of E1, which also supports the concept of better ease for anti-CEA – CEA association on the oxygen plasma treated bioreceptor interface. $\Delta G_{sorption}$ is reported for E1 at -6.1 ±0.36kcal mol^{-1} and that E2 at -6.6 ±0.52kcal mol^{-1}. These values are observed as higher than that of the previous studies reported similar experiments.[29,30] The negative $\Delta G_{sorption}$ values suggest favourable sorption process of CEA on the newly prepared SAM based bioreceptors surfaces. Additional evidence for the same has been determined through finding

the type of Langmuir sorption isotherm using the factor R_L, a dimensionless constant separation factor (L mmol^{-1}).

$R_L = 1 / (1 + bC_0)$ (15)

According to the concept if $R_L > 1$, the sorption unfavourable, while $0 < R_L < 1$, suggests a favourable conditions for sorption and $R_L = 0$, terms as irreversible reaction. The R_L values calculated for E1 reported in a region of 0.74 – 0.93 and that of E2 as 0.65 – 0.85 L mmol^{-1}.

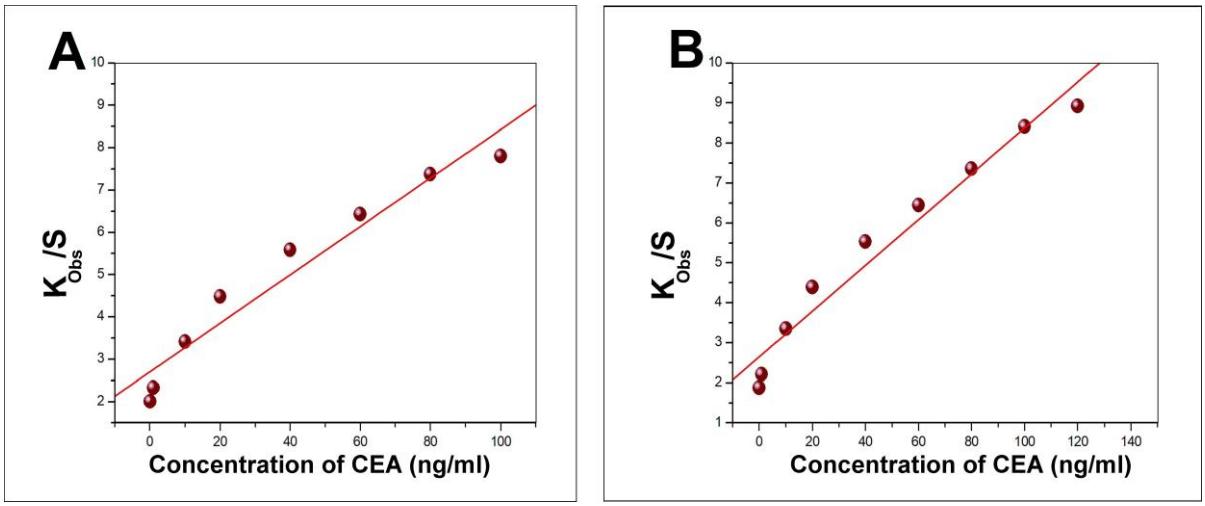

Figure 10(a) Representative Langmuir adsorption plot for the bioreceptors E1 and **(b)** E2

3.5. Long-term stability and selectivity of the biosensor

Selectivity of the biosensor was tested using other nonspecific proteins such as alpha-1-fetoprotein (AFP), cancer antigen 125 (CA125) and L-tryptophan. These proteins were added in different concentration to 1 ng/ml of CEA and the frequency response was recorded (Figure 11a and 11b). The performance of both the biosensors E1 and E2 finds free from the interference of nonspecific adsorption of other protein molecules presented in the sample solutions. The frequency response was recorded in a similar region as for the 1 ng/ml CEA stock solutions. However, the response time was delayed by 15-20 minutes as compared to the stock solution analysis. The combinations of protein solutions are listed in supportive data, Table S3. Long-term stability of the biosensor was tested by repeated immunoassay run with 1 ng/ml of CEA solution for 60 days. In a regular interval of 5 days the biosensor was tested and the results are given as the average values of variation in frequency shift for E1 and E2 in the Figure 11c and 11d respectively.

The biosensor receptors are stored at sterile conditions at 4°C after each immunoassay experiment. Regeneration of SAM was conducted through a glycine buffer solution run after each immunoassay experiment. During the initial 25 days of immunoassay run, the variation in frequency shift was recorded negligible and for another 10 days the variation was not more than 2-3% for E1. However, the variation in frequency response was increased steadily from 35th day onwards and at 60th day an average difference of 18% was recorded for the bioreceptor E1. On the other hand, E2 has recorded exceptionally high stability since till 40th the decrease in performance was negligible and a maximum of 17% decrease in efficiency was observed for E2 at the end of analysis period. The bioreceptor E2 has shown high resistivity towards the initiation in performance decrease till 40th day as compared to the bioreceptor E1. This may be due to the additional stability of the bioreceptor obtained through oxygen plasma treatment as proposed in the previous sections.

3.6. Real-time detection of clinical serum samples

The real-time application of the newly developed biosensor was examined using clinical serum samples. Total 10 serum samples were conducted immunoassay run using the biosensor and also tested through ELISA method. The collected samples are mainly from patients who are in the early stages of their colorectal cancer development. Prior to the measurement 0.5 mL of serum sample was added to 2 mL of PBS solution with pH 7.4. Further, the immunoassay run and calculation of deposited mass on the electrode surface was conducted as per the above-discussed methods. The results are depicted in Table 1 in comparison with the results obtained through the ELISA method. The study found no significant difference in the results given by the two methods. Also, the biosensor has reported better consistency in the results, which is proved by the smaller standard deviations values than ELISA results. Also, the response time is much faster for the biosensor (40-50 minutes) than that of ELISA method (6-8 hours).

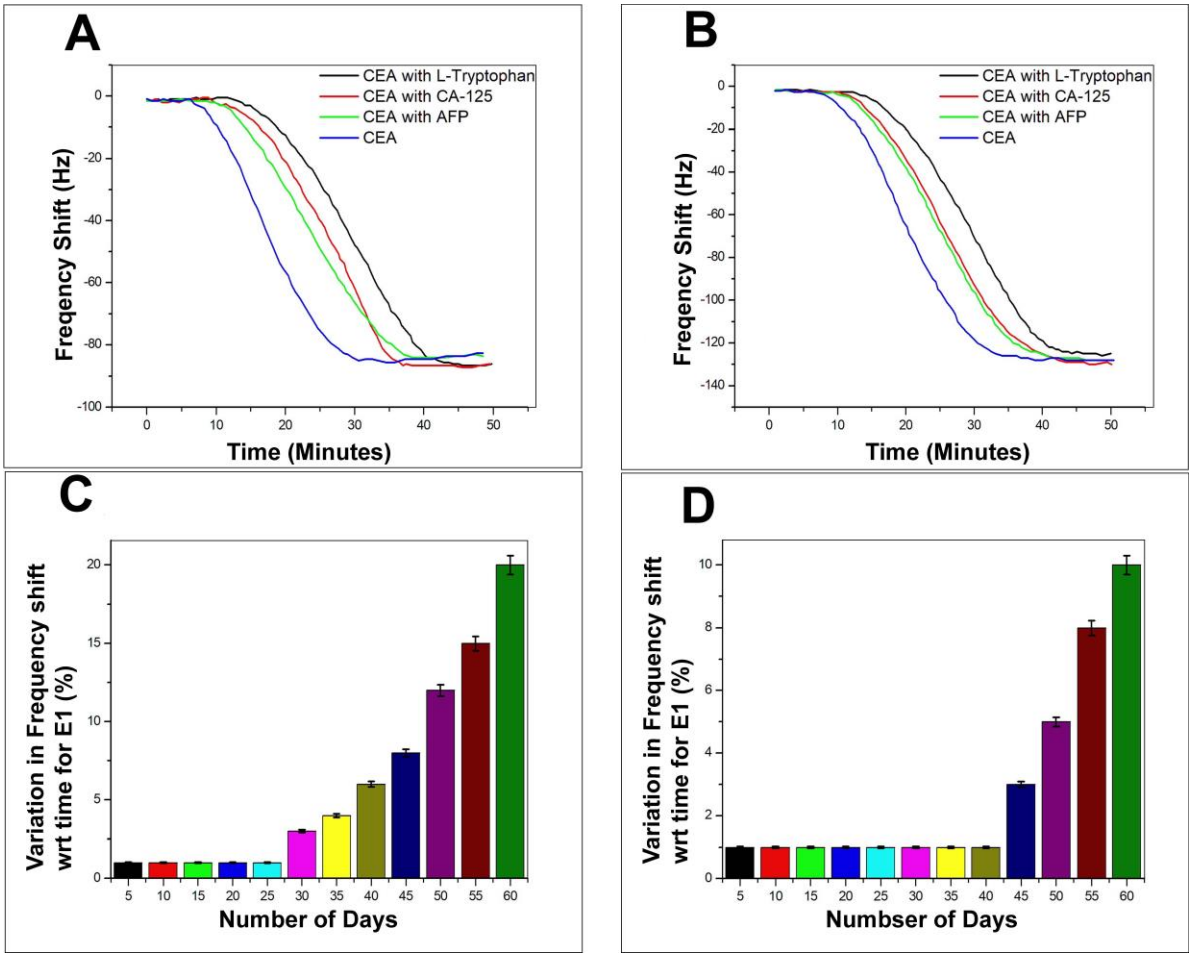

Figure 11(a) Immunoassay response during the selectivity study of the biosensors with various combinations of tumour marking proteins (Table S3) for E1 **(b)** E2 **(c)** Average values of the decrease in biosensing performance with time in terms of variation in frequency shift for E1 and **(d)** E2

Table 1: Clinical serum sample analysis results for bioreceptors E1 and E2 in comparison with ELISA method

No.	Biosensor E1 (ng/ml)	Biosensor E2 (ng/ml)	ELISA (ng/ml)
1	25.1±2.48	25.4±2.33	25.3±3.12
2	20.1±2.46	20.3±2.15	20.8±2.81
3	34.4±2.31	34.3±2.16	34.1±3.44
4	37.6±3.62	37.3±3.35	37.1±3.96
5	21.0±3.54	21.3±3.29	21.3±4.23
6	37.7±3.33	37.5±3.15	38.0±4.12
7	34.4±2.61	34.7±2.36	34.4±3.23
8	30.3±2.34	30.9±2.04	31.4±2.34
9	29.9±3.45	29.5±3.15	30.3±3.77
10	33.8±2.46	34.2±2.11	34.0±3.51

4. Conclusions

QCM biosensor for the real-time detection of CEA was successfully prepared through a SAM-based biosensor. The study proposes a simple, sensitive, efficient and highly selective piezoelectric immunosensing method for CEA detection and estimation. The limit of detection of the biosensor was estimated at 0.06 and 0.09 ng/ml of CEA concentration for the bioreceptors prepared through with and without oxygen plasma treatment respectively. The bioreceptors prepared through GO-AuNP coating on the QCM electrode by in-situ synthesis method and systematic integration of thioglycolic acid coupling unit through EDC-NHS reaction mechanism. Oxygen plasma treatment of electrode surface in the initial stage of bioreceptor preparation provided additional stability and sensitivity to the biosensor. Also, theoretical analysis using Langmuir sorption isotherm kinetics allowed to calculate k_a, k_d and ΔG during immunoassay run and suggested a stable bioreceptor – prey molecule interaction. The biosensor is suitable for multiple immunoassays run since the standard deviation of the test results found small and till 45^{th} day of biosensor preparation the decrease in biosensing efficiency was found less than 2%. The selectivity of the biosensor also was observed satisfactory with other common tumor marking proteins like AFP, CA125 and L-tryptophan. Clinical serum sample analysis has suggested that the biosensor as a promising method for the real-time detection of CEA. The test result was validated using the ELISA method and found comparable but with faster response time.
The conclusions section should come in this section at the end of the article, before the acknowledgements.

Conflicts of interest

The authors do not have any conflict of interest regarding this publication.

Acknowledgements

The authors gratefully acknowledge the support of Research and Development Program of China (Grant no. 2016YFB0402705). Project supported by State Key Laboratory of Powder Metallurgy, Central South University, Changsha, China, National Natural Science Foundation of China (NSFC Grant no. 11704261, 11575118), Shenzhen Science & Technology Project (Grant no. JCYJ20170817100658231, JCYJ20180507182439574 , JCYJ20180305124317872), Shenzhen Key Lab Fund (ZDSYS20170228105421966), UK Engineering and Physical Sciences Research Council (EPSRC) EP/P018998/1, Newton Mobility Grant (IE161019) from the UK Royal Society and the National Natural Science Foundation of China, and Royal Academy of Engineering UK-Research Exchange with China and India.

References

1. X. Gua, Z. Sheb, T. Mab, S. Tiana, H. B. Kraatz, Biosens. Bioelectron. 2018, **102**, 610–616.
2. Y. Wang, G. Zhao, Y. Zhang, X. Pang, W. Cao, B. Du, Q. Wei, Sens Actuators B Chem, 2018, **266**, 561–569.
3. H. Shu, W. Wen, H. Xiong, X. Zhang, S. Wang, Electrochem commun, 2013, **37**, 15–19.
4. O. Blixt, D. Bueti, B. Burford, D. Allen, S. Julien, M. Hollingsworth, A. Gammerman, I. Fentiman, J. Taylor-Papadimitriou, J. M. Burchell, Breast Cancer Res, 2011, **13**, 1-16.
5. Z. Qiu, J. Shu, J. Liu, D.Tang, Anal. Chem. 2019, **91**, 1260−1268.
6. Z. Yu, Y. Tang, G. Cai, R. Ren, D. Tang, Anal. Chem. 2019, **91**, 1222−1226.
7. P. Skladal, Piezoelectric biosensors, Trends Analyt Chem. 2016, **79**, 127-133.
8. J. Liao, M. Lu, D. Tang, Biochem Eng J, 2016, **114**, 276–282.
9. D. Tang, Q. Li, J. Tang, B. Su, G. Chen, Anal. Chim. Acta, 2011, **686**, 144–149.
10. J. W. Choi, B. S. Chun, B. K. Oh, W. Lee, W. H. Lee, Colloids Surf B Biointerfaces, 2005, **40**, 173-177.
11. X. Zhang, J. Chen, H. Liu, S. Zhang, Biosens. Bioelectron. 2015, **65**, 341–345.
12. X. Wang, H. Yu, D. Lu, J. Zhang, W. Deng, Sens Actuators B Chem, 2014, **195**, 630–634.
13. D. Chronaki, D. I. Stratiotis, A. Tsortos, E. Anastasiadou, E. Gizeli, Sens Biosensing Res, 2016, **11**, 99–106.
14. Z. G. Chen, D. Y Tang, Bioprocess Biosyst Eng, 2007, **30**, 243-249
15. X. Yang, R. Zhou, Y. Hao, P. Yang, Sci Bull, 2017, **62**, 923–930.
16. Y. Uludag, I. E. Tothill, Talanta, 2010, **82**, 277–282.
17. X. Yu, F. Chen, R. Wang, Y. Li, J Biotechnol, 2018, **266**, 39–49.
18. D. Tang, B. Zhang, J. Tang, L. Hou, G. Chen, Anal. Chem. 2013, **85**, 6958-6966.
19. Lingfeng Gao, Hongli Zhang, Hua Cui, Biosens. Bioelectron. 2014, **57**, 65-70.
20. Ylea Vlamidis, Isacco Gualandi, Domenica Tonelli, Journal of Electroanalytical Chemistry, 2017, **799**, 285-292.
21. Ronghui Wang, Lijun Wang, Zachary T. Callaway, Huaguang Lu, Tony Jun Huang, Yanbin Li, Sens Actuators B Chem, 2017, **240**, 934–940.
22. J. Kankare, Langmuir, 2002, **18**, 7092–7094.
23. Kenneth A. Marx, Biomacromolecules, 2003, **4**, 1099–1120.
24. B. D. Vogt, E. K. Lin, W. l. Wu, C. C. White, J Phys Chem B, 2004, **108**, 12685–12690.
25. T. Bürgi, Nanoscale, 2015, **7**, 15553-15567.
26. S. Li, Y. Wan, Y. Su, C. Fan, V.R. Bhethanabotla, Biosens. Bioelectron. 2017, **95**, 48-54.
27. M. Omidi, M. Choolaei, F. Haghiralsadat, M. Azhdari, N.D. Moghadam, F. Yazdian, Proceedings of the International Conference on Biomedical Electronics and Devices (BIODEVICES-2014), 2014, 134-139.
28. D. Zheng, J. Xiong, P. Guo, Y. Li, S. Wang, H. Gu, Mater Res Bull, 2014, **59**, 411-415.
29. M. Stobiecka, M. Hepel, Biosens. and Bioelectron. 2011, **26**, 3524-3530

30. D. S. Karpovich, G. J. Blanchard, Langmuir, 1994, **10**, 3315-3322.
31. M. Y. Emran, M. A. Shenashen, H. Morita, S. A. El-Safty, Biosens. and Bioelectron. 2018, **109**, 237–245.
32. M. Y. Emran , M. Mekawy , N. Akhtar , M. A. Shenashen, I. M. EL-Sewify, A. Faheem, S. A. El-Safty, Biosens. and Bioelectron.2018, **100**, 122–131.
33. M. Y. Emran, S. A. El-Safty, M. A. Shenashen, T. Minowa, Sens Actuators B Chem, 2019, **284**, 456–467.
34. M. Y. Emran, M. A. Shenashen, H. Morita, and S. A. El-Safty, Adv. Healthcare Mater. 2018, **7**, 1701459.